MNRAS

The thermal emission from boulders on (25143) Itokawa and implications for the YORP effect

P. Ševeček[1⋆], M. Brož[1], D. Čapek[2], J. Ďurech[1]
[1] *Institute of Astronomy, Charles University, Prague, V Holešovičkách 2, 18000 Prague 8, Czech Republic*
[2] *Astronomical Institute of the Academy of Sciences, Fričova 298, 251 65 Ondřejov, Czech Republic*

Accepted ???. Received ???; in original form ???

ABSTRACT
Infrared radiation emitted from an asteroid surface causes a torque that can significantly affect rotational state of the asteroid. The influence of small topographic features on this phenomenon, called the YORP effect, hasn't been studied yet in detail. In this work, we show that lateral heat diffusion in boulders of suitable sizes leads to the emergence of a local YORP effect which magnitude is comparable to the YORP effect due to the global shape. We solve a three-dimensional heat diffusion equation in a boulder and its surroundings by the finite element method using the FreeFem++ code. The contribution to the total torque is inferred from the computed temperature distribution. The general approach allows us to compute the torque induced by a realistic irregular boulder, including the influence of the global self-heating effect. For an idealized boulder, our result is consistent with an existing one-dimensional model. We estimated a size distribution of boulders on (25143) Itokawa, based on close-up images of surface. We realized that topographic features on Itokawa can induce a rotational acceleration of the order $10^{-7}\,\mathrm{rad/day^2}$ and can therefore explain the observed phase shift in light curves.

Key words: celestial mechanics – minor planets, asteroids – methods: ???.

1 INTRODUCTION

The Yarkovsky-O'Keefe-Radzievskii-Paddack effect is the torque caused by the infrared emission from an asteroidal surface and its impact on a rotational state of an asteroid (Rubincam 2000). It is now widely recognized as an important factor, affecting the evolution of rotational states of asteroids alongside mutual collisions and tidal torques. The YORP effect helped to explain numerous observed phenomenona, such as a spin axis alignment of asteroids in the Korinis family (Vokrouhlický et al. 2003), a non-maxwellian rotational frequency distributions of small main-belt asteroids (Pravec et al. 2008) or significant binary asteroid population among near-Earth objects (Walsh et al. 2012).

Even a *direct* evidence of a non-gravitational torque has been found. A phase shift in light curves has been measured for a few asteroids that can't be explained by a solely gravitational model — (1862) Apollo (Kaasalainen et al. 2007), (54509) YORP (Lowry et al. 2007; Taylor et al. 2007), (1620) Geographos (Ďurech et al. 2008), (3103) Eger (Ďurech et al. 2012) and finally, (25143) Itokawa (Lowry et al. 2014).

The asteroid Itokawa has been a suitable candidate for a detection of YORP effect for its highly asymmetric shape and its favourable position among near-Earth objects. Vokrouhlický et al. (2004) predicted a measurable accelaration of rotation of the order of $10^{-7}\,\mathrm{rad/day^2}$, based on the shape model derived by radar ranging. Itokawa was a target of the Hayabusa spacecraft in 2005 and a state-of-the-art shape model of the asteroid was constructed from silhouette images (Gaskell et al. 2006). The torque computed using the latter model would lead to a significant deceleration $-(1.8 \text{ to } 3.3) \cdot 10^{-7}\,\mathrm{rad/day^2}$ (Scheeres et al. 2007). However, the measured phase shift in light curves revealed *acceleration* $+(3.54 \pm 0.38) \cdot 10^{-8}\,\mathrm{rad/day^2}$ (Lowry et al. 2014). Theoretical models didn't predict even the sign of the effect correctly. This discrepancy between observed and predicted change of the angular frequency hasn't been fully explained to date.

The observed rotational acceleration could be atributed to density inhomogeneities in the asteroid. Scheeres and Gaskell (2008) showed that the YORP effect on Itokawa is indeed sensitive to the position of the center of mass. Based on the measured acceleration, Lowry et al. (2014) computed the required offset between the center of mass and the center of figure to be $\sim 21\,\mathrm{m}$. Such offset indicates that the asteroid might consist of two parts with different densities — $(2850 \pm 500)\,\mathrm{kg/m^3}$ and $(1750 \pm 110)\,\mathrm{kg/m^3}$. On the other hand, the surface of the asteroid appears rather uniform.

⋆ E-mail: pavel.sevecek@gmail.com

The differences in boulder distributions on the two parts do not seem statistically significant (Mazrouei et al. 2014).

The deceleration predicted by Scheeres et al. (2007) was computed from the shape model with $\sim 50\,000$ facets. Calculations of the effect with a more detailed shape lead to an even bigger deceleration. Furthermore, with increasing resolution the deceleration doesn't show any sign of a convergence, implying that even sub-meter sized surface features possibly have a non-negligible influence (Breiter et al. 2009).

There is a problem that shapes with surface features of sub-meter sizes cannot be easily included in existing models of the YORP effect. There are several reasons for this limitation. First, numerical YORP models typically assume that temperature changes only in the direction perpendicular to the surface (i.e. a plane-parallel approximation). This assumption allows a solution of the one-dimensional heat diffusion equation for each surface facet independently. This is well justified as long as surface features are significantly larger then the diurnal thermal skin depth, with varies from mm to dm (Vokrouhlický and Brož 1999). This assumption is no longer applicable for a high-resolution shape model and a full three-dimensional solution of the heat diffusion equation is required. Second, no shape is described to the required level of detail. So far, the best shape model is that of the asteroid Itokawa. The model in the best available resolution consists of over 3 million facets, which corresponds to meter-sized surface features.

As Golubov and Krugly (2012) pointed out, surface features of sizes comparable to the thermal skin depth could potentially have significant influence on the total YORP effect. They considered a stone wall (an idealized boulder) located on the equator of a spherical asteroid and aligned with a local meridian. The wall was assumed to be high enough so that the heat would be mostly conducted in a transverse direction and the heat diffusion equation can be solved using the one-dimensional approximation. They demonstrated that the emission from the surface of the wall can create a torque that won't vanish after averaging over the rotational period. Assuming a large number of such "walls" placed along the equator, the corresponding torque is comparable to the torque arising from the global-shape asymmetry of certain asteroids, scaled to equivalent diameter.

The goal of this paper is to solve the heat diffusion equation in a *realistic* boulder and infer the total torque boulders contribute to the YORP effect on the asteroid Itokawa. The problem requires a numerical solution in a general three-dimensional mesh, which we construct using the `TetGen` code (Si 2006). We solve the heat diffusion equation using the finite element method, which is suitable for irregular domains, utilizing the `FreeFem++` code (Hecht 2012). Our model includes the influence of shadows casted by the boulder and the global self-heating effect from thermal emission and scattered radiation.

possible extensions? => future works

Contents

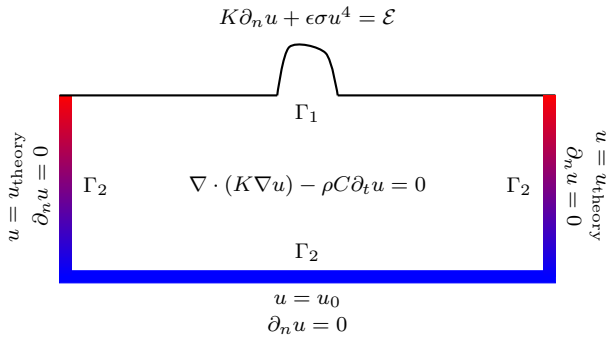

Figure 1. The domain and boundary conditions of the problem. The examined boulder constitutes the top of the domain Ω. Coloured strips indicate the surface Γ_2, where the temperature is held fixed by Dirichled boundary conditions. The temperature distribution inside the domain and on the surface Γ_1 is computed numerically, solving the heat diffusion equation (2) and the energy balance equation (3).

2 THE HEAT DIFFUSION EQUATION AND A WEAK FORMULATION OF THE PROBLEM

Our problem may be specified as follows. We search for a temperature $u(\vec{r}, t)$ inside the boulder and its surroundings, i.e. an unknown scalar function on a domain Ω. The differential operator corresponding to the heat diffusion equation (HDE) is:

$$\mathcal{L} \equiv \rho C \partial_t - \nabla \cdot K \nabla \,, \tag{1}$$

where K denotes the thermal conductivity, ρ the density, C the specific heat capacity of the material. The function u thus has to fulfill the relation:

$$\mathcal{L}(u) = 0 \,. \tag{2}$$

At the same time, we require the boundary conditions to be met at the boundary of the domain $\partial\Omega$. The boundary consists of two surfaces, which we denote Γ_1 and Γ_2, as shown in Figure 1.

The surface Γ_1 represents the surface of the asteroid, the boundary condition is the energy balance equation

$$K\partial_n u + \epsilon\sigma u^4 = \mathcal{E} \,, \tag{3}$$

where ∂_n denotes a derivative along the normal, ϵ the infrared emissivity, σ the Stefan–Boltzmann constant, $\mathcal{E}$ the total incoming radiative flux. The boundary $\partial\Omega$ is a non-convex surface, thus the radiative heat exchange also contributes to the total flux $\mathcal{E}$ (i.e. the global self-heating effect). We denote the solar flux $\mathcal{E}_\odot$ and the flux incoming from visible parts of the surface — the thermally emitted flux and the scattered flux — as $\mathcal{E}_{\mathrm{rad}}$ and $\mathcal{E}_{\mathrm{sc}}$ respectively. The total flux is the sum $\mathcal{E} = \mathcal{E}_\odot + \mathcal{E}_{\mathrm{rad}} + \mathcal{E}_{\mathrm{sc}}$. Summands can be expressed as

$$\mathcal{E}_\odot = (1 - A)\Phi\mu\vec{s} \cdot \vec{n} \,, \tag{4}$$

$$\mathcal{E}_{\mathrm{rad}} = (1 - A) \int_{\Gamma_1} \epsilon' \sigma u'^4 \frac{\cos\vartheta \cos\vartheta'}{\|\vec{r} - \vec{r}'\|} \nu \,\mathrm{d}\Gamma' \,, \tag{5}$$

$$\mathcal{E}_{\mathrm{sc}} = (1 - A) \int_{\Gamma_1} A' \Phi \mu' \vec{s} \cdot \vec{n}' \frac{\cos\vartheta \cos\vartheta'}{\|\vec{r} - \vec{r}'\|} \nu \,\mathrm{d}\Gamma' \,, \tag{6}$$

where A is the Bond albedo, Φ the flux of solar radiation,

$\vec{s}$ the body–Sun direction, $\vec{n}$ the outward normal to the surface, $\vec{r}$ the position vector, ϑ the angle between the local normal and the direction vector connecting points $\vec{r}$ and $\vec{r}'$, μ the shadowing function, ν the visibility function. The prime denotes a value of a quantity at the point of surface element $\mathrm{d}\Gamma'$. We assume the Lambert's cosine law for the intensity of thermal emission and scattered radiation, hence the $\cos\vartheta'$ in equations (5) and (6).

The shadowing function μ is defined on the surface Γ_1. The value of $\mu(\vec{r})$ equals 1 if the point $\vec{r}$ is insolated, 0 if it lies in the shadow. The visibility function ν is defined on $\Gamma_1 \times \Gamma_1$. We assign the value of function $\nu(\vec{r},\vec{r}')$ to 1 if points $\vec{r}$ and $\vec{r}'$ have a visual contact, 0 otherwise. In most cases, the value of ν is simply $\nu(\vec{r},\vec{r}') = H(\vec{n}\cdot(\vec{r}-\vec{r}'))H(\vec{n}'\cdot(\vec{r}'-\vec{r}))$, where H is the Heaviside step function and $\vec{n}$, $\vec{n}'$ denotes the local normal at point $\vec{r}$, $\vec{r}'$ respectively.

The boundary Γ_1 is defined by a set of triangular facets S_i. Integrals in equations (5) and (6) can be therefore computed by a formal substitution $\int_{\Gamma_1}\mathrm{d}\Gamma' \to \sum_i S_i$. We also restrict values of the shadowing function μ and the visibility function ν to whole facets. This restriction gives rise to an error; however, it can be limited substantially by choosing a high-resolution surface mesh.

We also need to specify boundary conditions on the surface Γ_2, which goes through the interior of the asteroid, closing the boundary $\partial\Omega$. It can be selected arbitrarily; we choose the shape corresponding to five walls of a block, which is a convenient choice as we can simply set a zero-flux boundary condition

$$K\partial_n u = 0\,. \tag{7}$$

This condition will be met as long as dimensions of the domain Ω are significantly greater than dimensions of the boulder. The influence of the boulder can be considered negligible at large distances. At sides of the domain, the temperature will only change in the direction perpendicular to the surface, the dot product of the normal vector and the temperature gradient will therefore be null. At a great depth, the temperature will be effectively constant, which means the temperature gradient at the bottom of the domain will be null, satisfying the boundary condition (7).

We are going to solve the HDE numerically, using a finite-element discretization in space. In this approach, the function u is approximated by (Langtangen 2003):

$$u \doteq \hat{u} = \sum_{j=1}^{M} u_j N_j\,, \tag{8}$$

where N_j denote prescribed basis functions, u_j unknown coefficients we search for and M corresponds to the number of vertices defined on the domain. Since $\hat{u}$ is only an approximation of u, applying the PDE operator would generally yield a non-zero result:

$$\mathcal{L}(\hat{u}) \neq 0\,, \tag{9}$$

nevertheless, we require the integral of all residua over the domain to be zero:

$$\int_\Omega \mathcal{L}(\hat{u}) W_i \mathrm{d}\Omega = 0\,, \tag{10}$$

where W_i are suitable weighting (test) functions. This is called a *weak formulation* of the problem. In the Galerkin method, the test functions are simply the basis functions, $W_i \equiv N_i$, so that

$$\int_\Omega \mathcal{L}(\hat{u}) N_i \mathrm{d}\Omega = 0\,. \tag{11}$$

Essentially, it constitutes a system of M equations for u_j coefficients.

In our case of the HDE (Eq. 2):

$$\int_\Omega \rho C \partial_t \hat{u} N_i \mathrm{d}\Omega - \int_\Omega \nabla\cdot(K\nabla\hat{u}) N_i \mathrm{d}\Omega = 0\,. \tag{12}$$

The second term may be rewritten according to the Green lemma as:

$$\int_\Omega \nabla\cdot(K\nabla\hat{u}) N_i \mathrm{d}\Omega = -\int_\Omega K\nabla\hat{u}\cdot\nabla N_i \mathrm{d}\Omega + \oint_{\partial\Omega} K\partial_n\hat{u} N_i \mathrm{d}\Gamma, \tag{13}$$

which enables to incorporate the boundary condition easily, because we can express the normal derivative from boundary conditions (3) and (7), that is $K\partial_n\hat{u} = -\epsilon\sigma\hat{u}^4 + \mathcal{E}$ on Γ_1, $K\partial_n\hat{u} = 0$ on Γ_2.

Regarding the temporal derivative, we use a finite-difference discretization:

$$\partial_t\hat{u} \simeq \frac{\hat{u}^n - \hat{u}^{n-1}}{\Delta t}\,. \tag{14}$$

and an implicit Euler scheme, so that we plug $\hat{u}^n$ in the remaining terms, whenever possible. The only exception is the non-linear radiative term, where we perform a linearization

$$\hat{u}^4 \simeq \hat{v}^3\hat{u} \tag{15}$$

and we employ an iterative method to find a solution. The $\hat{v}$ denotes a solution of a previous iteration. In some cases, the iterative method does not converge, thus we introduce the relaxation parameter ω. In each iteration, we find the solution $\hat{u}_*$ of the linear problem and then assign the new value of $\hat{u}$ by taking the linear combination of current and previous solution

$$\hat{u} = \omega\hat{u}_* + (1-\omega)\hat{v}\,. \tag{16}$$

We achieved convergence for all considered values of parameters by selecting $\omega = 0.6$

+ initial condition

The final equation is thus:

$$\int_\Omega \frac{\rho C}{\Delta t}\hat{u}^n N_i \mathrm{d}\Omega - \int_\Omega \frac{\rho C}{\Delta t}\hat{u}^{n-1} N_i \mathrm{d}\Omega + \int_\Omega K\nabla\hat{u}^n\cdot\nabla N_i \mathrm{d}\Omega + \\ + \int_{\Gamma_1} \epsilon\sigma v^3 \hat{u}^n N_i \mathrm{d}\Gamma - \int_{\Gamma_1} \mathcal{E}\mathrm{d}\Gamma = 0\,. \tag{17}$$

We actually need not to substitute for $\hat{u}$ from Eq. (8) or express the corresponding matrices, because this is done automatically by the FreeFem++ code. We use a conjugate gradient method, which is suitable for sparse linear systems.

3 THE MEAN TORQUE CAUSED BY AN IRREGULAR BOULDER

The magnitude of a recoil force varies during rotational period and revolution of an asteroid around the Sun. A long-term effect of the force is therefore given by its time-averaged value. We follow the assumption of Golubov and Krugly (2012) and consider an asteroid on a circular orbit with zero

obliquity. Although the YORP effect depends on the obliquity in a non-trivial way (Čapek and Vokrouhlický 2004), the zero obliquity allows us to average the recoil force over a rotational period only.

The direct radiation pressure has a negligible influence on the YORP effect (Nesvorný and Vokrouhlický 2008), we therefore consider the scattered radiation and the thermal emission. We assume the Lambert's cosine law for the intensity of scattered and emitted radiation. The recoil force from the surface element $\mathrm{d}S$ is then

$$\mathrm{d}\vec{f}_{\mathrm{rad}} = -\frac{2}{3}\frac{A\Phi}{c}\mu(\vec{s}\cdot\vec{n})\vec{n}\mathrm{d}S\,, \tag{18}$$

$$\mathrm{d}\vec{f}_{\mathrm{sc}} = -\frac{2}{3}\frac{\epsilon\sigma}{c}u^4\vec{n}\mathrm{d}S\,. \tag{19}$$

The total torque caused by the boulder is given by the surface integral over the boulder

$$\vec{T} = \int_{\Gamma_1}\vec{r}\times\mathrm{d}\vec{f}\,. \tag{20}$$

The direction of a torque is generally different from the axis of rotation $\vec{e}$. Both the direction and the magnitude of the torque depends on exact shape of the boulder. However, even a symmetric boulder can induce a non-zero torque due to the lateral heat diffusion. The torque is caused by the asymmetry of emission from the eastern side and western side of the boulder, therefore it will have the direction of the rotational axis $\vec{e}$.

3.1 The coordinate system and the parameters of the problem

We choose a topocentric coordinate system centered on a studied boulder. The z axis has therefore a direction of a local normal, x axis is aligned with a meridian and y axis completes a right-handed orthogonal Cartesian system.

We introduce quantities that help us reduce a number of independent parameters of the problem. We define the subsolar temperature

$$u_\star = \sqrt[4]{\frac{(1-A)\Phi}{\epsilon\sigma}}\,, \tag{21}$$

the diurnal thermal skin depth

$$L = \sqrt{\frac{2K}{\omega\rho C}}\,, \tag{22}$$

where ω is the angular frequency of the asteroid, and the thermal parameter

$$\Theta = \frac{\sqrt{K\omega\rho C}}{4\sqrt{2}\pi^{-\frac{3}{4}}\epsilon\sigma u_\star^3}\,. \tag{23}$$

Numerical constants in these definitions arise from the derivation of the analytical solution (see Appendix A), it should be noted that some authors don't include them (Lagerros 1996; Golubov and Krugly 2012).

If we neglect self-heating terms, the heat diffusion equation (2) and its boundary condition (3) can be rewritten using dimensionless variables $\vec{\xi} = \vec{r}/L$, $\varphi = \omega t$, $\tau = u/u_\star$ as

$$\frac{1}{2}\Delta_\xi\tau - \frac{\partial\tau}{\partial\varphi} = 0\,, \tag{24}$$

$$4\pi^{-\frac{3}{4}}\Theta\vec{n}\cdot\nabla_\xi\tau + \tau^4 = \vec{s}\cdot\vec{n}\,, \tag{25}$$

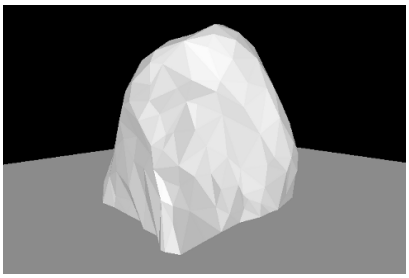

Figure 2. The shape of a boulder used as a domain for a solution of HDE.

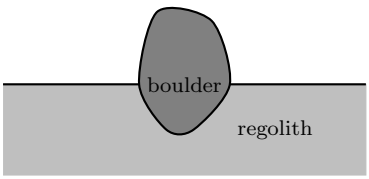

Figure 3. The domain of the solution Ω is divided into two parts of different thermal conductivities. Thermal properties of a regolith are given by Farinella et al. (1998).

where ∇_ξ, Δ_ξ is the gradient and the Laplacian with respect to the variables ξ. The only independent parameter in these equations is the thermal parameter Θ. However, the boundary condition must hold for all $L\vec{\xi} \in \partial\Omega$. If ℓ is the characteristic size of the boulder, then the problem of finding a dimensionless temperature τ has two independent parameters — thermal parameter Θ and the dimensionless size ℓ/L.

3.2 The numerical solution of the heat diffusion equation

We solve the weak formulation of the HDE (17) by a finite element method. For the domain of the solution, we choose the studied boulder and its surroundings. The shape of the boulder can be arbitrary; the boulder we chose for computations is shown on image 2. As a special case, we can choose the high wall and compare our results to the model of Golubov and Krugly (2012), see Appendix **??**.

We considered different values of thermal conductivity for the studied boulder and for the surrounding layer of regolith, as demonstrated in Figure 3. Thermal properties of the regolith are given by Farinella et al. (1998), properties of the boulder are determined by values of thermal parameter Θ and skin depth L.

We should stress the importance of *non-linearity* of the problem. We derived a linearized analytical solution of the heat diffusion equation in half-space domain (see Appendix A), where we deal with the non-linear term u^4 by substituting $u_0^4 + 4u_0^3\delta u$, where u_0 is a constant, δu is the change of temperature. Same term appears in the expression for the recoil force (18) from a thermal emission. In case of a symmetric boulder, the linearization of the problem would lead to identically zero mean torque.

The solution of the HDE is a time-dependent temperature distribution in the boulder, particularly on its surface. We can therefore determine the recoil force the boulder ex-

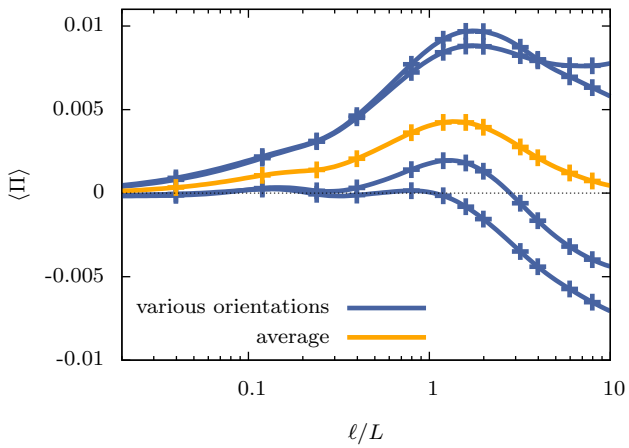

Figure 4. Computed values of the mean dimensionless pressure $\langle\Pi\rangle$ as a function of the dimensionless boulder size ℓ/L. Blue curves correspond to the boulder rotated by 0 °, 90 °, 180 ° and 270 °. We notice that all curves show zero limit for $\ell/L \to 0$, as well as maximum for $\ell \sim L$. The orange curve is the arithmetic mean of blue curves.

erts. The force is given by the formula (18); however, it is convenient to introduce the dimensionless pressure

$$\Pi = \frac{2}{3}\frac{1}{S}\int_{\Gamma_1}\frac{u^4}{u_\star^4}n_y\,\mathrm{d}\Gamma \tag{26}$$

where n_y is the y-th component of the local normal, S is the base area of the boulder. The dimensionless pressure allows us to compare the magnitude of the tangential force for different sizes of the boulder. The projection of the total torque to the rotational axis is then given by

$$\vec{T}\cdot\vec{e} = \frac{(1-A)\Phi}{c}\Pi S r\cos\vartheta\,, \tag{27}$$

where $r\cos\vartheta$ is the distance of the boulder from the rotational axis.

Consider a wall aligned with a local meridian, which face of area S has a constant temperature u. The definition (26) is then reduced to

$$\Pi = \frac{2}{3}\frac{u^4}{u_\star^4}\,, \tag{28}$$

which is the definition of a dimensionless pressure by Golubov and Krugly (2012). Our definition can be therefore viewed as a generalization.

The dimensionless pressure varies during a rotation. We obtain a parameter describing a long-term effect by averaging over one rotational period, thus we introduce the mean dimensionless pressure

$$\langle\Pi\rangle = \frac{1}{P}\int_0^P \Pi\,\mathrm{d}t\,. \tag{29}$$

3.3 The invariant pressure from the set of various orientations of the boulder

The mean dimensionless pressure $\langle\Pi\rangle$ as a function of the dimensionless size ℓ/L varies significantly for different shapes of a boulder, or even for different orientations of the same boulder. It is evident that the limit of very high conductivity (that is $\ell/L \to 0$) leads to a zero dimensionless pressure Π for *all* shapes of a boulder. In such case, the boulder is isothermal and therefore emits the same radiant flux to the western and eastern direction, resulting in a null torque.

The limit of the mean dimensionless pressure for zero thermal conductivity differs from boulder to boulder. The conductive term in the energy balance equation (3) is negligible and the temperature at a given point of a surface is determined by the immediate balance between incoming and outgoing radiant flux. Since we solve the HDE in a single boulder, we need to obtain a torque (as a function of a boulder size) that would represent all boulders on the surface. If we imagine boulders as wedges, it is reasonable to assume that the wedges will be randomly oriented on the surface. Although some orientations of boulders seems to be preffered on certain parts of the surface of Itokawa (Miyamoto et al. 2007), we anticipate that no orientaion prevails on the global scale. The total torque induced by boulders will therefore vanish in the limit of zero conductivity. For that reason, we demand the mean torque $\langle\Pi\rangle$ to approach zero as well. However, in the general case of an asymmetric boulder, the mean dimensionless pressure will approach a non-zero value.

We have several options how to resolve this issue. For instance, we can restrict the model to symmetric boulders only. If the boulder is symmetric with respect to a plane of a local meridian, the mean pressure will vanish in the limit case. Nonetheless, we want to maintain the universality of the model and use the irregular asymmetric boulder. In this case, we can compute the mean pressure $\langle\Pi\rangle$ for several orientations of the boulder and then take the average of these values. Another possibility is to calculate the mean pressure for a single orientation and subtract the pressure in the limit of zero conductivity. We employed the former option.

The Figure 4 shows the mean dimensionless pressure for several orientations of the studied boulder as well as averaged values. We chose the thermal parameter $\Theta = 0.5$ and assumed the boulder lies on the equator of an asteroid.

3.4 A dependence of the mean pressure on asteroidal latitude

For an asteroid with zero obliquity, the body-Sun vector $\vec{s}$ has Cartesian coordinates

$$\vec{s} = (\sin\vartheta\cos t, -\sin t, -\cos\vartheta\cos t)\,, \tag{30}$$

where t is the hour angle and ϑ is the asteroidal latitude. The dependence of the dimensionless pressure Π on the hour angle t vanishes after averaging over a period, the dependence on ϑ remains.

Assuming we can separater variables ℓ, ϑ, we can write the mean pressure $\langle\Pi\rangle$

$$\langle\Pi\rangle(\ell,\vartheta) = \mathcal{P}(\ell)\mathcal{V}(\vartheta)\,, \tag{31}$$

where $\mathcal{P}(\ell) = \langle\Pi\rangle(\ell,0)$. The function $\mathcal{V}(\vartheta)$ constitutes a latitude dependence and is normalized such that $\mathcal{V}(0\,^\circ) = 1$. It obviously depends on the shape of a boulder. We chose approximately hemisherical boulder, because it is axially symmetric and thus doesn't prefer one latitude over other values.

We show computed values of function $\mathcal{V}(\vartheta)$ in Figure 5. It can be approximated by a function $\cos a\vartheta$, where $a = 0.653 \pm 0.004$ is a constant determined by a least square

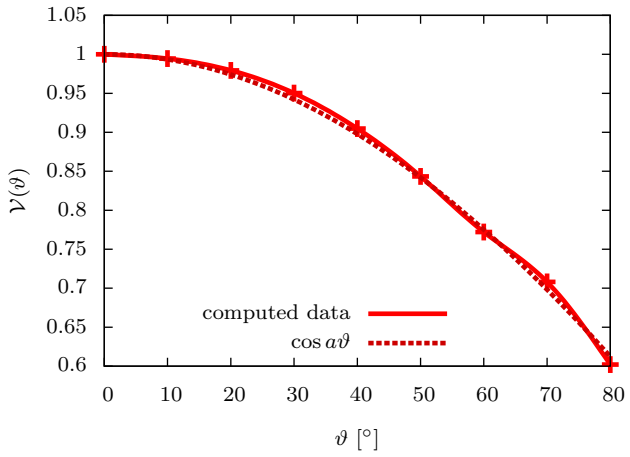

Figure 5. The dependence of the mean dimensionless pressure $\langle\Pi\rangle$ on the asteroidal latitude ϑ.

method. The mean pressure $\langle\Pi\rangle$ seems to be maximal for boulders on the equator.

4 THE ANGULAR ACCELERATION OF THE ASTEROID (25143) ITOKAWA

In the following, we focus our attention on the asteroid (25143) Itokawa. We estimate the number of boulders on the surface and show how the thermal emission from boulders alters the angular acceleration predicted by global-shape models of the YORP effect.

Existing models of the YORP effect usually assume the normal direction of the recoil force. For non-convex asteroid, the force can be influenced by the absorption of emitted radiation by the surface (Statler 2009). In previous chapter, we showed that surface feature can alter the recoil force as well. We pointed out that the lateral heat diffusion through boulders leads to emergence of the *tangential* component of the recoil force. The presence of tiny surface features change the normal component as well, the complete solution would require solving the heat diffusion equation in whole asteroid, including boulders. However, we neglect the change in normal component and solve the tangential component separately.

The torque generated by a single boulder was discussed in previous chapter. We place a large number of such boulders on the shape model of Itokawa and calculate the torque they induce. The total YORP torque and corresponding change in angular velocity of the asteroid is then obtained by adding our result to the result of the global-shape model of the YORP effect.

4.1 The torque induced by boulders

Let $\delta T(\vec{r},\ell)$ be the torque caused by single boulder of a size ℓ at position $\vec{r}$, $N(\ell)\mathrm{d}\ell$ the number of boulders on the surface of the asteroid with size in interval $(\ell,\ell+\mathrm{d}\ell)$, $\ell_{\min}$ and $\ell_{\max}$ the assumed minimal size of the boulder, maximal size respectively, and finally $\mathcal{D}$ the "boulder spatial distribution function". Then the total torque caused by boulders is given by

$$T=\int_{\partial\Omega}\int_{\ell_{\min}}^{\ell_{\max}}\delta T(\vec{r},\ell)N(\ell)\mathcal{D}(\vec{r})\,\mathrm{d}\ell\,\mathrm{d}\Gamma\,. \tag{32}$$

As the boundary of Itokawa is represented by the set of n triangular facets, we can write

$$T=\sum_{i=1}^{n}\mathcal{D}_i S_i\int_{\ell_{\min}}^{\ell_{\max}}\delta T(\vec{r}_i,\ell)N(\ell)\,\mathrm{d}\ell\,, \tag{33}$$

where S_i is the area of i-th facet, $\vec{r}_i$ its position vector, $\mathcal{D}_i$ spatial distribution coeficient such that $\sum_i\mathcal{D}_i=(\sum_i S_i)^{-1}$. We assume boulder size distribution $N(\ell)$ is independent on a location on the surface. Let $N(\ell)=N_{\mathrm{tot}}\varrho(\ell)$, where N_{tot} is the total number of boulders and $\varrho(\ell)$ is the probability density function. Then we can write

$$T=N_{\mathrm{tot}}\sum_{i=1}^{n}\mathcal{D}_i S_i E[\delta T(\vec{r}_i)]\,, \tag{34}$$

where $E[\cdot]$ is the expected value. Assuming boulder spatial distribution is isotropic ($\mathcal{D}_i=\mathrm{const.}$), we obtain a recipe for computing a total torque

$$T=\frac{N_{\mathrm{tot}}}{S}\sum_{i=1}^{N}S_i E[\delta T(\vec{r}_i,\ell)]\,, \tag{35}$$

where $S=\sum_i^n S_i$ is the surface area of the asteroid.

4.2 The observed size distribution of small boulders

In order to obtain the torque caused by boulders, it is necessary to find out the total number of boulders and their size distribution. The differential size distribution of boulders larger than 5 m on whole surface of Itokawa can be approximated by power law (Saito et al. 2006)

$$N(\ell)\mathrm{d}\ell\approx 1.3\cdot 10^5\cdot[\ell]_{\mathrm{m}}^{-3.8}\mathrm{d}\ell\,. \tag{36}$$

Surface images taken by the Hayabusa spacecraft revealed that the power law (36) can be extrapolated down to sizes of 1 dm on certain parts of the surface (Miyamoto et al. 2007), although the slope of a log-log graph falls significantly for smaller sizes. However, other parts of surface clearly shows different topography. Furthermore, extrapolation of the above mentioned size distribution down to 1 mm is unacceptable. Boulders of sizes between 1 mm and 1 dm alone would take about $4\cdot 10^7\,\mathrm{m}^2$, but the surface of Itokawa is only $3.93\cdot 10^5\,\mathrm{m}^2$ (Demura et al. 2006).

Therefore, we sought for a different size distribution of small pebbles. We estimated the size distribution from close-up images taken by the Hayabusa during its descend, namely images ST_2563537820_v and ST_2563607030_v. The resolution of these images is 7 mm/pixel, 6 mm/pixel respectively, which allows us to find distinct boulders only few centimeters in size. Identified boulders are shown on Figure 6. We constructed histogram of sizes (see Figure 7). Applying the least squares method, we get the power law

$$N(\ell)\,\mathrm{d}\ell=(3.9\pm 1.8)\cdot 10^5\cdot[\ell]_{\mathrm{m}}^{-(2.4\pm 0.3)}\,\mathrm{d}\ell\,. \tag{37}$$

The slope of ~ -2.4 is indeed much lower than the slope ~ -3.8 of the power law (36). We assume the power law (37) can be extrapolated to milimeter-sized pebbles. This assumtion is plausible as the total area of small pebbles does not

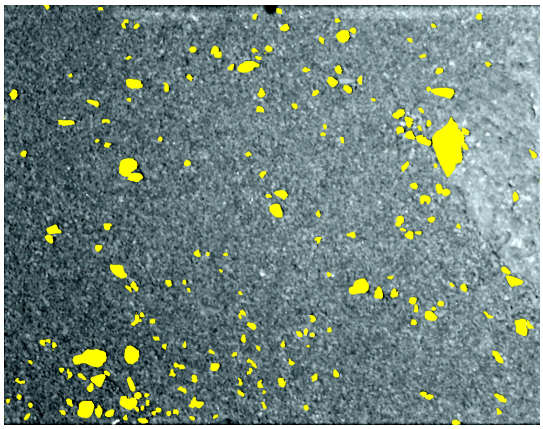

Figure 6. The image ST_2563607030_v with highlighted boulders from which we derived the size distribution used for computation of the total torque.

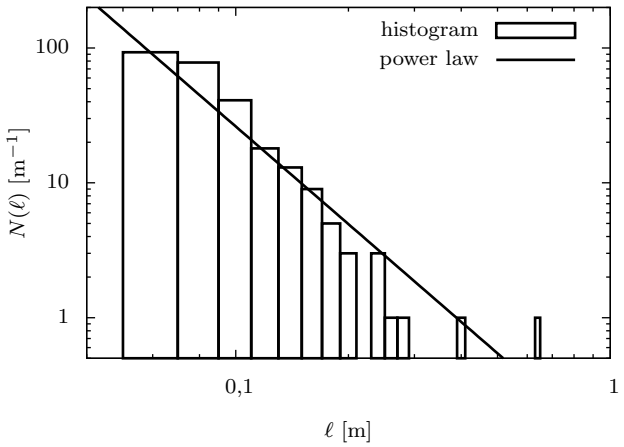

Figure 7. The histogram of small boulder sizes on the surface of Itokawa, constructed from images ST_2563537820_v and ST_2563607030_v.

diverge — the power law exponent is lower than 3. Neglecting uncertainties, pebbles of sizes between 1 mm and 1 dm would take about $1.5 \cdot 10^5\,\mathrm{m}^2$, which is about 40 % of the Itokawa surface.

4.3 The integration of the local effect to the global-model prediction

The global-shape YORP effect model of the asteroid Itokawa predicts a significant rotational deceleration, which is inconstistent which an observed acceleration. As mentioned above, the lateral heat diffusion through boulders induces an additional torque, which affects the change of angular velocity. Let the magnitude of the total torque generated by boulders be T, as given by equation (35). The asteroid will undergo rotational acceleration

$$\frac{\mathrm{d}\omega}{\mathrm{d}t} = \left(\frac{\mathrm{d}\omega}{\mathrm{d}t}\right)_{\mathrm{global}} + \frac{T}{I}\,, \qquad (38)$$

where $(\mathrm{d}\omega/\mathrm{d}t)_{\mathrm{global}}$ is the prediction of the global-shape YORP model, $I \doteq 7.77 \cdot 10^{14}\,\mathrm{kg\,m}^2$ is the moment of inertia of Itokawa (Scheeres et al. 2007).

The global-shape model of the YORP effect predicts the rotational deceleration $-(2 \text{ to } 6) \cdot 10^{-7}\,\mathrm{rad/day}^2$, depending on the resolution of the shape model (Breiter et al. 2009). In order to determine the torque induced by boulders, it is necessary to select values of the parameters — the thermal parameter Θ and the thermal skin depth L. We selected $\Theta = 0.5$, $L = 0.01\,\mathrm{m}$.

Utilizing the size distribution of boulders derived in the section 4.2, we obtain a result

$$\frac{T}{I} = (4.6 \pm 2.2) \cdot 10^{-7}\,\mathrm{rad/day}^2 \qquad (39)$$

The error is given by the multiplicative constant of the power law (37).

We notice that the result is comparable to the result of the global-shape model in magnitude, but has an opposite sign. The torque induced by boulders and the torque from the global asymmetry could effectively cancel out, resulting in the change of angular velocity much smaller than predicted by global-shape models. Remarkably, the observed angular acceleration of Itokawa is $(3.54 \pm 0.38) \cdot 10^{-8}\,\mathrm{rad/day}^2$ (Lowry et al. 2014), which is a value constistent with our findings. Our model therefore presents an alternative explanation of observed acceleration.

5 CONCLUSIONS

We presented the numerical model of the local YORP effect, induced by a boulder. The three-dimensional heat diffusion equation in the boulder was solved using the finite element method. Unlike the finite difference method, the finite element method has basically no restriction on the shape of a domain, allowing us to solve the heat diffusion equation in the boulder of a realistic shape. Furthermore, we assumed the studied boulder has a different thermal conductivity than the surrounding layer of regolith. We adopted thermal values of regolith from Farinella et al. (1998).

The studied boulder had a general asymmetric shape, so it showed a non-zero torque even in the limit of zero thermal conductivity. However, this limit torque depends on the orientation of the boulder. In order to obtain an invariant torque representing all boulders, we computed a torque for several orientations and then found the average of these values. We showed that the averaged torque approaches zero in the zero conductivity limit.

The non-zero torque arise from the asymmetry of the emission indicatrix (averaged over the rotational period). There are two "sources" of the emission asymmetry. The first is the asymmetry of the boulder shape. Rubincam (2000) demonstrated the emergence of the YORP effect on the toy model of a spherical asteroid with two wedges attached to its equator. The torque created by the emission from the vertical wall is greater in magnitude than the torque created by the emission from the inclined wall, thus resulting in a non-zero total torque. The second source of the emission asymmetry comes from the lateral heat diffusion through the boulder. Imagine a boulder on the equator. In the morning, the eastern side of the boulder is heated up and the boulder exerts a recoil force of western direction. If the width

of the boulder is comparable to the thermal skin depth, the heat diffusion contributes to heating of the western side in the afternoon. The emission from the western side is therefore more intense. The recoil force has an eastern direction and exceeds the force from eastern side in magnitude, thus creating a non-zero mean force of eastern direction. The corresponding torque causes the acceleration of the asteroid.

We pointed out that the global contribution of the shape asymmetry of boulders to the YORP effect is likely to be null, because of the very large number of boulders on the surface. In contrast, the lateral heat diffusion leads to the torque with a direction of the rotational axis, thus accumulating over individual boulders. Even though the torque generated by a single boulder is tiny, the overall effect can be comparable to the global-shape effect, if there is sufficient amount of boulders.

The general approach allowed us to compare our model with the one-dimensional model of Golubov and Krugly (2012). In case of a *symmetric* boulder, we confirmed that the torque vanishes in the limit of high conductivity and zero conductivity, and also for both slow and fast rotating bodies. Introducing the thermal parameter Θ and the thermal skin depth L, we showed that the maximum torque appears for $\Theta \sim 1$, $L \sim 1$.

Unlike Golubov and Krugly (2012), we found positive values of the torque for all values of parameters in case of symmetric boulder. The asymmetric boulder can produce negative torque, but after averaging over orientations the resulting torque is again strictly positive. Nevertheless, even Golubov and Krugly (2012) realized the torque is mostly positive, and proposed the posibility of a equilibrium between the global-shape torque and the torque induced by boulders, resulting in a null total torque. They suggested this could be the case of the asteroid (25143) Itokawa; however, Lowry et al. (2014) detected the positive change in angular velocity of Itokawa, which means the asteroid is not in the equilibrium state.

Our model contains number of free parameters that can change the magnitude of the effect significantly. The crucial factor is the total number of boulders and the size distribution. We showed that the size distribution of large boulders on Itokawa cannot be extrapolated to centimeter sizes. For lack of a better alternative, we estimated the size distribution from close-up images of the surface of Itokawa and extrapolated it for sizes of indiscernible pebbles. We also assumed that other parts of the surface have the same size distribution of boulders. Based on this size distribution, boulders of sizes between 1 mm and 1 dm would occupy about 40 % of the surface of Itokawa. Provided we neglect an interaction of boulders (mutual shadowing, irradiation), the torque is directly proportional to the number of boulders.

The choice of the lower limit of the power-law size distribution is also a disputable parameter. Although the magnitude of the torque induced by a boulder approaches zero as the size of the boulder approaches zero, even sum-milimeter pebbles could have a non-negligible influence on the total torque. However, it is doubtful whether so small particles can be considered as boulders, or whether they form a uniform layer of matter. We selected the lower limit 1 mm.

The shape of the studied boulder is anothey key factor of our model. We selected a boulder of a realistic irregular shape, but it was selected ad hoc. Particularly important properties of boulders are their height and their flatness. The higher the boulder is, the greater torque it is likely to induce. If the walls of the boulder are perpendicular to the surface, the lever arm of the torque is maximal. The lower the slope of walls, the lower lever arm.

We applied the computed torque to a case of the asteroid (25143) Itokawa. We showed that boulders could induce a torque that would cause the acceleration $(4.6 \pm 2.2) \cdot 10^{-7}\,\mathrm{rad/day^2}$. We realize the uncertainty of our result; nevertheless, we demonstrated that the emission from boulders *is capable* of producing the torque comparable to the global-shape YORP effect. Models of global YORP effect on asteroid Itokawa predict significant deceleration $\mathrm{d}\omega/\mathrm{d}t = -(2 \text{ to } 6) \cdot 10^{-7}\,\mathrm{rad/day^2}$, where the value varies with the shape resolution used (Breiter et al. 2009). The observed change in angular frequency is $\mathrm{d}\omega/\mathrm{d}t = (3.54 \pm 0.38) \cdot 10^{-8}\,\mathrm{rad/day^2}$ (Lowry et al. 2014). Simply by adding the local and the global values, we arrive to the result that is consistent with the observed acceleration, thus present an alternative explanation beside the shift in center of mass by Lowry et al. (2014).

We assumed the rotational axis perpendicular to the orbital plane, therefore we don't have to consider the orbital movement and the torque is averaged over the rotational period only. The obliquity of Itokawa is approximately 178 ° (Demura et al. 2006), which is very close to the perpendicular state. Considering the general direction of the rotational axis, the insolation will change during the revolution over the Sun and the seasonal changes of temperature occurs. We expect the seasonal variant of the studied effect to appear on boulders whose size is comparable to the seasonal thermal skin depth.

We discussed the diurnal torque has a direction of the rotational axis, as it is caused by the asymmetry of emission between the western and the eastern part of the boulder due to the lateral heat diffusion. Following the same principle, the seasonal torque could be caused by the asymmetry between the northern and the southern part of the boulder. The direction of the torque would therefore be perpendicular to the rotational axis. We anticipate the seasonal component of the effect won't affect the change in angular velocity of an asteroid; at the most, it will cause an evolution of the rotational axis. Our model cannot estimate the magnitude of the seasonal component, a future research is required.

Future works ??

6 ACKNOWLEDGEMENTS

The work of MB has been supported by the Grant Agency of the Czech Republic (grant no. 13-01308S) and the Research Programme MSM0021620860 of the Czech Ministry of Education.

REFERENCES

Breiter, S., Bartczak, P., Czekaj, M., Oczujda, B., Vokrouhlický, D., Nov. 2009. The YORP effect on 25143 Itokawa. Astronomy and Astrophysics 507, 1073–1081.

Čapek, D., Vokrouhlický, D., Dec. 2004. The YORP effect with finite thermal conductivity. Icarus 172, 526–536.

Demura, H., Kobayashi, S., Nemoto, E., et al., 2006. Pole and global shape of 25143 Itokawa. Science 312, 1347–1349.

Ďurech, J., Vokrouhlický, D., Kaasalainen, M., et al., 2008. Detection of the YORP effect in asteroid (1620) Geographos. Astronomy and Astrophysics 489, 25–28.
Ďurech, J., Vokrouhlický, D. Kaasalainen, M., Higgins, D., et al., Nov. 2012. Analysis of the rotation period of asteroids (1865) Cerberus,(2100) Ra-Shalom, and (3103) Eger-search for the YORP effect. Astronomy and Astrophysics 547, 10.
Farinella, P., Vokrouhlický, D., Hartmann, W. K., Apr. 1998. Meteorite Delivery via Yarkovsky Orbital Drift. Icarus 132, 378–387.
Gaskell, R., Saito, J., Ishiguro, M., et al., 2006. Global Topography of Asteroid 25143 Itokawa. In: 37th Annual Lunar and Planetary Science Conference. Vol. 37. p. 1876.
Golubov, O., Krugly, Y. N., Jun. 2012. Tangential Component of the Yorp Effect. The Astrophysical Journal 752, 11.
Hecht, F., 2012. New development in FreeFem++. Journal of numerical mathematics 20, 251–265.
Kaasalainen, M., Ďurech, J., Warner, B. D., Krugly, Y. N., Gaftonyuk, N. M., Mar. 2007. Acceleration of the rotation of asteroid 1862 Apollo by radiation torques. Nature 446, 420–422.
Lagerros, J., Jun. 1996. Thermal physics of asteroids. I. Effects of shape, heat conduction and beaming. Astronomy and Astrophysics 310, 1011–1020.
Langtangen, H. P., 2003. Computational Partial Differential Equations. Numerical Methods and Diffpack Programming. Springer-Verlag, Berlin.
Lowry, S. C., Fitzsimmons, A., Pravec, P., et al., Oct. 2007. Direct Detection of the Asteroidal YORP Effect. Science 39, 415.
Lowry, S. C., Weissman, P. R., Duddy, S. R., et al., Feb. 2014. The internal structure of asteroid (25143) Itokawa as revealed by detection of YORP spin-up. Astronomy and Astrophysics 562, 48.
Mazrouei, S., Daly, M., Barnouin, O., Ernst, C., DeSouza, I., Feb. 2014. Block distributions on Itokawa. Icarus 229, 181–189.
Miyamoto, H., Yano, H., Scheeres, D. J., et al., May 2007. Regolith migration and sorting on asteroid Itokawa. Science 316, 1011–1014.
Nesvorný, D., Vokrouhlický, D., Mar. 2008. Vanishing torque from radiation pressure. Astronomy and Astrophysics 480, 1–3.
Pravec, P., Harris, A., Vokrouhlický, D., et al., Oct. 2008. Spin rate distribution of small asteroids. Icarus 197, 497–504.
Rozitis, B., Green, S. F., Jun. 2012. The influence of rough surface thermal-infrared beaming on the Yarkovsky and YORP effects. Monthly Notices of the Royal Astronomical Society 423, 367–388.
Rubincam, D., Nov. 2000. Radiative Spin-up and Spin-down of Small Asteroids. Icarus 148, 2–11.
Saito, J., Miyamoto, H., Nakamura, R., et al., Jun. 2006. Detailed images of asteroid 25143 Itokawa from Hayabusa. Science 312, 1341–1344.
Scheeres, D., Gaskell, R., Nov. 2008. Effect of density inhomogeneity on YORP: The case of Itokawa. Icarus 198, 125–129.
Scheeres, D. J., Abe, M., Yoshikawa, M., et al., 2007. The effect of YORP on Itokawa. Icarus 188, 425–429.
Si, H., 2006. TetGen - A Quality Tetrahedral Mesh Generator and Three-Dimensional Delaunay Triangulator. http://tetgen.berlios.de/.
Statler, T. S., Aug. 2009. Extreme sensitivity of the YORP effect to small-scale topography. Icarus 202, 502–513.
Taylor, P. A., Margot, J.-L., Vokrouhlicky, D., et al., 2007. Spin rate of asteroid (54509) 2000 PH5 increasing due to the YORP effect. Science 316, 274–277.
Vokrouhlický, D., Brož, M., Oct. 1999. An improved model of the seasonal Yarkovsky force for regolith-covered asteroid fragments. Astron. Astrophys. 350, 1079–1084.
Vokrouhlický, D., Nesvorný, D., Bottke, W., Sep. 2003. The vector alignments of asteroid spins by thermal torques. Nature 425, 147–151.
Vokrouhlický, D., Čapek, D., Kaasalainen, M., Ostro, S. J., 2004. Detectability of YORP rotational slowing of asteroid 25143 Itokawa. Astronomy and Astrophysics 24, 21–24.
Walsh, K. J., Richardson, D. C., Michel, P., Aug. 2012. Spin-up of rubble-pile asteroids: Disruption, satellite formation, and equilibrium shapes. Icarus 220, 514–529.

APPENDIX A: A LINEARIZED ANALYTICAL SOLUTION OF THE ONE-DIMENSIONAL HEAT DIFFUSION EQUATION

The general three-dimensional heat diffusion equation with a non-linear boundary condition in an irregular domain has no analytical solution. To find the temperature distribution we must employ a numerical method, such as the finite element method. However, it is useful to derive an analytical solution for simplified case of a half-space domain, which allows to reduce the problem to only one spatial dimension. The solution can be used as a test for the numerical model and also as a Dirichlet boundary condition (see ??).

(Lagerros 1996)

Suppose the Sun illuminates (infinite) plane $z = 0$ and a half-space $z > 0$ represents the domain. We seek for the temperature u as a function of depth z and time t, solving the heat diffusion equation

$$\frac{\partial^2 u}{\partial z^2} - \frac{1}{\alpha}\partial_t u = 0 \tag{A1}$$

with a boundary conditions

$$-K\frac{\partial u}{\partial z}(0,t) + \epsilon\sigma u^4(0,t) = \mathcal{E}(t)\,, \tag{A2}$$

$$\frac{\partial u}{\partial z}(\infty,t) = 0\,, \tag{A3}$$

where $\alpha = \frac{K}{\rho C}$ is the thermal diffusivity, K the thermal conductivity, ρ the density, C the specific heat capacity, ϵ the emissivity, σ the Stefan-Boltzmann constant and $\mathcal{E}(t)$ the incoming radiant flux. The first boundary condition is the energy balance equation and the second for definite (jednoznacne ??) solution — it eliminates the solution where the temperature rises ad infinitum as $z \to \infty$.

The radiant flux is a periodic function, therefore we can represent it as a Fourier series $\mathcal{E}(t) = \sum_{n=-\infty}^{\infty} \mathcal{E}_n e^{in\omega t}$. We look for a *stationary* solution, which we can represent by the sum $u(z,t) = \sum_{n=-\infty}^{\infty} u_n(z) e^{in\omega t}$. Substituing into (A1) and applying the constraint (A3) we obtain the solution

$$u_0(z) = a_0\,, \tag{A4}$$

$$u_n(z) = a_n e^{-(1+i)\beta_n z}\,, \tag{A5}$$

$$u_{-n}(z) = a_{-n} e^{(i-1)\beta_n z}\,, \tag{A6}$$

where $\beta_n \equiv \sqrt{\frac{|n|\omega}{2\alpha}}$. We determine constants a_n from the boundary condition (A2). Here we run into problems with the non-linear term u^4.

$u^4 \approx u_0^4 + 4u_0^3 \sum_{n\neq 0} u_n e^{in\omega t}$

The thermal parameter of the n-th mode $\Theta_n = \frac{K\beta_n}{4\epsilon\sigma u_0^3}$ and the phase offset $\tan\varphi_n = -\left(\frac{\Theta_n}{\Theta_n+1}\right)\operatorname{sgn} n$

We can choose the initial time arbitrarily, we choose $\mathcal{E}(t) = (1-A)\Phi\Xi(\cos\omega t)$ where $\Xi(x) = x$ for $x \geqslant 0$, $\Xi(x) = 0$ for $x < 0$. First six Fourier modes are $\mathcal{E}(t) \approx (1-A)\Phi\left(\frac{1}{\pi} + \frac{1}{2}\cos\omega t + \frac{2}{3\pi}\cos 2\omega t - \frac{2}{15\pi}\cos 4\omega t + \frac{2}{35\pi}\cos 6\omega t\right)$

$$u(z,t) = \sqrt[4]{\frac{\mathcal{E}_0}{\epsilon\sigma}} + \sum_{n=1}^{\infty} \frac{\mathcal{E}_n}{2\epsilon\sigma u_0^3} \frac{e^{-\beta_n z}\cos\left(n\omega t - \beta_n z + \varphi_n\right)}{\sqrt{2\Theta_n^2 + 2\Theta_n + 1}}\,. \tag{A7}$$

APPENDIX B: VARIANTS OF THE INSOLATION FUNCTION AND COMPARISON WITH EXISTING ONE-DIMENSIONAL MODEL

APPENDIX C: THE ERROR ESTIMATE OF THE FINITE ELEMENT METHOD

This paper has been typeset from a TEX/ LATEX file prepared by the author.